

A new precise mass for the progenitor of the Type IIP SN 2008bk^{★†‡}

Justyn R. Maund^{1,2§}, Seppo Mattila³, Enrico Ramirez-Ruiz⁴ & John J. Eldridge⁵

¹ *Astrophysics Research Centre, School of Mathematics and Physics, Queen's University Belfast, Belfast, BT7 1NN, Northern Ireland*

² *Royal Society Research Fellow*

³ *Finnish Centre for Astronomy with ESO (FINCA), University of Turku, Väisäläntie 20, FI-21500 Piikkiö, Finland*

⁴ *Department of Astronomy & Astrophysics, University of California, Santa Cruz, 95064, U.S.A.*

⁵ *Department of Physics, University of Auckland, Private Bag 92019, Auckland, New Zealand*

18 November 2021

ABSTRACT

The progenitor of the Type IIP SN 2008bk was discovered in pre-explosion $g'r'i'YJHK_s$ images, acquired with European Southern Observatory Very Large Telescope FORS, HAWK-I and ISAAC instruments and the Gemini GMOS-S instrument. The wealth of pre-explosion observations makes the progenitor of this SN one of the best studied, since the detection of the progenitor of SN 1987A. Previous analyses of the properties of the progenitor were hampered by the limited quality of the photometric calibration of the pre-explosion images and the crowded nature of the field containing the SN. We present new late-time observations of the site of SN 2008bk acquired with identical instrument and filter configurations as the pre-explosion observations, and confirm that the previously identified red supergiant star was the progenitor of this SN and has now disappeared. Image subtraction techniques were used to conduct precise photometry of the now missing progenitor, independently of blending from any nearby stars. The nature of the surrounding stellar population and their contribution to the flux attributed to the progenitor in the pre-explosion images are probed using *HST* WFC3 UVIS/IR observations. In comparison with MARCS synthetic spectra, we find the progenitor was a highly reddened RSG with luminosity $\log(L/L_\odot) = 4.84^{+0.10}_{-0.12}$, corresponding to an initial mass of $M_{\text{init}} = 12.9^{+1.6}_{-1.8} M_\odot$. The temperature of the progenitor was hotter than previously expected for RSGs ($T \sim 4330\text{K}$), but consistent with new temperatures derived for RSGs using SED fitting techniques. We show that there is evidence for significant extinction of the progenitor, possibly arising in the CSM; but that this dust yields a similar reddening law to dust found in the ISM ($E(B - V) = 0.77$ with $R_V = 3.1$). Our improved analysis, which carefully accounts for the systematics, results in a more precise and robust mass estimate, making the progenitor of SN 2008bk the most well understood progenitor of a Type IIP SN from pre-explosion observations.

Key words: supernovae:general – supernovae:individual (2008bk)

1 INTRODUCTION

All single stars with initial masses in the range $8 \lesssim M_{\text{init}} \lesssim 25 - 30 M_\odot$ are predicted to end their lives as Red Supergiants (RSGs). These stars are expected to end their evolution with a core-collapse induced supernova (SN) explosion; with the massive H-rich envelope, retained by the RSG, giving rise to the characteristic light curve plateau and H-dominated spectra of Type IIP SNe.

Although there have been efforts to infer the properties of the progenitor star through interpreting the observed characteristics of the subsequent SN (e.g. Utrobin & Chugai 2008; Dessart et al. 2013), the direct observation of the progenitor in fortuitous pre-explosion images has provided direct constraints on the properties of the progenitors independently of models of how SNe explode (for a review see Smartt 2009). The greatest success in the direct detection of the progenitors has been for the Type IIP SNe, originating from

[★] Based on observations collected for program 087.D-0587 at the European

Organisation for Astronomical Research in the Southern Hemisphere, Chile

[†] Based on observations obtained for program GS-2011B-Q-21 at the

Gemini Observatory, which is operated by the Association of Universities

for Research in Astronomy, Inc., under a cooperative agreement with the

NSF on behalf of the Gemini partnership: the National Science Founda-

tion (United States), the National Research Council (Canada), CONICYT

(Chile), the Australian Research Council (Australia), Ministério da Ciência,

Tecnologia e Inovação (Brazil) and Ministerio de Ciencia, Tecnología e In-

novación Productiva (Argentina)

[‡] Based on observations made with the NASA/ESA Hubble Space Tele-

scope, which is operated by the Association of Universities for Research in

Astronomy, Inc., under NASA contract NAS 5-26555. These observations

are associated with program GO-12262.

[§] j.maund@qub.ac.uk

RSGs (Smartt et al. 2009). An analysis of the population of observed and undetected progenitors with mass constraints, showed that Type IIP SNe appear to only arise from progenitor stars in the mass range $8 < M_{\text{init}} \lesssim 16 M_{\odot}$, implying that RSGs evolving from more massive stars were either exploding as a different type of SN or, perhaps, not exploding as observable SNe. Smartt et al. (2009) referred to the observed deficit of massive RSG progenitors as the “RSG problem”.

Recently, Walmswell & Eldridge (2012) and Kochanek et al. (2012) have explored the role of dust in the circumstellar mediums (CSMs) of RSGs progenitors, in addition to foreground Galactic and host reddening components, in dimming the most massive and luminous progenitors ($\geq 15 M_{\odot}$), causing the masses determined for these RSGs to be systematically under-estimated (Walmswell & Eldridge 2012). The determination of the masses of the progenitor stars of Type IIP SNe have, however, relied on observations of fortuitous nature. These observations are often shallow and have limited wavelength coverage. The direct assessment of the roles of multiple reddening components have, therefore, been undermined by the degeneracies between the different parameters (in particular reddening and temperature) which cannot generally be broken with the available data and which, therefore, have serious consequences for the determination of the luminosity and mass of the progenitors.

The application of Spectral Energy Distribution (SED) techniques to progenitor stars detected in pre-explosion images provides a robust method to evaluate the degeneracies between parameters and quantitatively explore the consequences of additional reddening components. Maund et al. (2013) showed, using MARCS synthetic spectra, that previous observations of the progenitors of Type IIP SNe were not consistent with large amounts of CSM dust with composition and reddening law significantly different to dust in the interstellar medium (ISM). This could imply that dust may not be a solution to the RSG problem.

SN 2008bk was discovered by Monard (2008) on 2008 Mar 25.14, which Li et al. (2008) subsequently placed 9.2’’E and 126.4’’N of the centre of the host galaxy NGC 7793. Li et al. also identified a possible red star close to the position of SN 2008bk in the pre-explosion images, for which Maoz & Mannucci (2008) reported European Southern Observatory (ESO) Very Large Telescope (VLT) ISAAC J and K_s photometry. Previously Mattila et al. (2008) and Van Dyk et al. (2012) have presented the full identification and parameterisation of the progenitor, independently determining the initial mass of the progenitor to be 8.5 ± 1 and $8 - 8.5 M_{\odot}$, respectively. Mattila et al. (2010) later reported the subsequent disappearance of the progenitor, confirming the identity of the red supergiant observed in pre-explosion images.

Due to the wealth of multi-wavelength pre-explosion observations, the progenitor of SN 2008bk presents the opportunity to provide the best constraints for the progenitors of any SN since SN 1987A (Gilmozzi et al. 1987). Here we present new late-time observations of the site of SN 2008bk, acquired with the Gemini South Telescope, the European Southern Observatory Very Large Telescope (VLT) and the Hubble Space Telescope to open a new window onto the nature of the progenitor object.

In Section 2 we present the new late-time observations of the site of SN 2008bk and their reduction. The results of these new observations are presented in Section 3, and the outcome of our extensive analysis is represented in Section 4. In Section 5 we present a discussion of our results and our conclusions.

2 OBSERVATIONS & DATA REDUCTION

The details of the pre-explosion, post-explosion and late-time images used here are presented in Table 1.

2.1 VLT FORS, HAWK-I and ISAAC Observations

The pre-explosion ESO VLT FORS, HAWK-I and ISAAC observations were previously presented by Mattila et al. (2008) (the near-infrared images were also used by Van Dyk et al. 2012). Late-time VLT observations of the site of SN 2008bk were acquired with almost identical instrument configurations as the pre-explosion observations, as part of program 087.D-0587 (PI Maund); these late-time VLT observations were acquired under photometric conditions. The near-infrared HAWK-I and ISAAC late-time observations were acquired using identical instrument configurations as the pre-explosion observations ~ 3.4 yrs after explosion. The late-time FORS observations were acquired with a close approximation of the instrument configuration used for the pre-explosion observations: the pre-explosion observations utilised the FORS1 instrument with the Tektronix detector providing a pixel scale of 0.2’’, whereas the late-time observations used the newly designated FORS instrument (originally FORS2) with the red optimised MIT detectors providing a pixel scale 0.252’’ (Appenzeller et al. 1998). The data were reduced using the corresponding ESO pipelines¹.

The FORS data were bias and flatfield corrected in the standard fashion. The infra-red HAWK-I and ISAAC data were bias, flat corrected and sky subtracted (using interleaved sky offset frames) before combination. Photometry of the late-time frames was conducted using IRAF and the Point Spread Function (PSF) fitting routines in the daophot package. The data were photometrically calibrated with zeropoints, colour terms and extinction coefficients derived from observations of standard fields, acquired on the same nights.

The pre-explosion and late-time FORS observations were conducted with the Bessell BVI filters, but the corresponding zeropoints and colour terms were used to place the photometry in the Johnson-Cousins BVI photometric system. The HAWK-I and ISAAC data were similarly calibrated using observations of infrared standard stars in the $YJHK_s$ filters. The JHK_s zeropoints were checked against photometry of bright stars in the late-time images that were also in the 2MASS point source catalogue, with a corresponding dispersion of 0.03, 0.08 and 0.1 magnitudes, respectively. The pre-explosion photometry was bootstrapped to the photometric calibration of the late-time images.

2.2 Gemini GMOS-S Observations

The pre-explosion Gemini GMOS-S observations were previously presented by Van Dyk et al. (2012). We attempted to re-identify the data used by Van Dyk et al. in the Gemini archive², according to the description of observations provided by Van Dyk et al.. The data were reduced in the standard fashion using IRAF and the specific gemini data reduction package³. The data were bias and flatfield corrected, and the individual chips for each exposure were combined to produce mosaiced images. The mosaic images were coadded to produce deep images for each filter. The pre-explosion

¹ <http://www.eso.org/sci/software/pipelines/>

² <http://www3.cadc-ccda.hia-ihp.nrc-cnrc.gc.ca/gsa/>

³ <http://www.gemini.edu/node/10795>

observations were conducted in filters close to the Sloan Digital Sky Server (SDSS) $g'r'i'$ filters, but were conducted under non-photometric conditions.

Late-time observations Gemini GMOS-S were conducted with an identical instrument setup, under improved seeing and photometric conditions compared to the pre-explosion observations, ~ 3.5 yrs post-explosion as part of program GS-2011B-Q-21 (PI Maund). The data were reduced in the same fashion as the pre-explosion Gemini observations. Photometry of the images was conducted using IRAF and Point-Spread Function fitting routines in the daophot package. The i' observations were conducted under photometric conditions, and the photometric zeropoint was calibrated using observations of photometric standards on the same night, assuming standard colour and extinction terms. The g' and r' observations were also conducted under photometric conditions, however conditions degraded later in the night and it was not possible to observe a photometric standard. Using observations of photometric standards acquired in an interval spanning 5 days either side of 2011 Sep 21, we have established that the g' and r' photometric zeropoints are stable, with the error on the weighted mean zeropoint of 0.005 magnitudes. The calibrated g' , r' and i' photometry was originally in the AB magnitude system and was converted to Vega magnitudes with the addition of the constants +0.102, -0.165 and -0.403 mags, respectively, derived through synthetic photometry of the spectrum of Vega (Bohlin & Gilliland 2004).

2.3 Late-time HST WFC3 UVIS & IR imaging

Additional late-time observations of the site of SN 2008bk were acquired with the HST Wide Field Camera 3 Ultraviolet-Visible (UVIS) and Infrared (IR) Channels, with the F814W, F125W and F160W filters. The observations were acquired as part of program GO-12262 (PI Maund). For each filter, four separate exposures in a four-point box dither pattern. The separate exposures were combined using the multidrizzle package, running under PyRAF, to achieve better sampling than the native pixel scale affords from a single pointing. The observations were conducted using the smaller 1024×1024 and 512×512 pixel subarrays of the UVIS2 and IR detectors. The UVIS F814W image was drizzled to a final pixel scale of $0.025'' \text{ px}^{-1}$, while the IR observations were drizzled to a final pixel scale of $0.078'' \text{ px}^{-1}$. Photometry of the images was conducted using daophot, running as part of IRAF. Empirical aperture corrections were determined to final aperture sizes of $0.4''$, and the standard Vegamag zero points were adopted⁴. The UVIS2 F814W image was further corrected for Charge Transfer Inefficiency using the calibration of Noeske et al. (2012), following the scheme outlined by Annibali et al. (2008) and Maund et al. (2013). As there were no corresponding pre-explosion HST images, the late-time observations were used to probe the nature of the underlying background flux that may have contributed to the pre-explosion ground-based observations.

2.4 Differential Astrometry

The position of the SN in the pre-explosion and late-time images was determined using differential astrometry with respect to the position of the SN observed in a post-explosion VLT NACO adaptive-optics K_S image (presented by Mattila et al. 2008). Transformations between the post-explosion K_S image and the late-time images

were calculated using the IRAF task geomap. The post-explosion image was used to directly determine the position of the SN on the late-time $i'YJHK_S$ images; and the positions on the i' and I images were further used to determine the SN position on the $g'r'$ and BV images respectively. The SN position on the pre-explosion frames was determined using transformations calculated between the pairs of late-time and pre-explosion images with the same filters.

2.5 Detection limits & artificial star tests

In each image, where objects of interest were not detected, the detection threshold was determined using artificial star tests. Artificial stars were placed in the images, at the positions where the detection thresholds were to be determined, utilising the PSFs derived from previous stages of photometry with daophot. Recovery of the artificial stars was then attempted using daophot in the same configuration used for the original photometry of the images. The completion function for the recovery of the artificial stars, as a function of magnitude, was approximated by a cumulative normal distribution, with mean at 50% completeness and the standard deviation corresponding to the breadth of the function.

2.6 ISIS image subtraction

Following Maund & Smartt (2009), we use the image subtraction package ISIS (Alard & Lupton 1998; Alard 2000) to subtract the late-time images from the pre-explosion images, to derive precise photometry of the now absent progenitor object. The late-time images were transformed to match the coordinate system of the pre-explosion images; as the late-time images were generally taken under better seeing conditions than the pre-explosion images, this resulted in a slight degradation of image quality of the late-time images, but still better than the pre-explosion images. The late-time images were then used as the template frames to be subtracted from the pre-explosion images, except in the case of ISAAC J and K_S frames for which the pre-explosion images were acquired under better seeing. Aperture photometry was conducted on the residuals in the difference image, as part of the ISIS package (this was checked against aperture photometry with daophot, and the differences were found to be negligible). The zeropoint was determined relative to aperture photometry of non-varying stars in the same field and their photometry derived using daophot (see section 2). Although ISIS derives the usual statistical uncertainties from aperture photometry, the additional systematic uncertainty in using ISIS was estimated by conducting multiple iterations of the image subtraction process with the settings modified. This allowed us to quantify the effect of various parameters, such as: the number of stamps used to calculate the convolution kernel to match the PSFs of the template and input images; the degree of the fit to the background; the degree of the spatial variability of the kernel; and the size of the aperture and background annulus used for the photometry of the residuals.

3 RESULTS

The pre-explosion, late-time and difference images of the site of SN 2008bk are presented for the VLT FORS, Gemini GMOS and VLT HAWK-I and ISAAC observations in Figs. 1, and 2 and 3, respectively. The late-time HST observations are presented in Fig. 4. Photometry of the pre-explosion and late-time images is presented

⁴ http://www.stsci.edu/hst/wfc3/phot_zp_lbn

Table 1. Pre-explosion, post-explosion and late-time observations of the site of SN 2008bk

Date (UT)	Telescope+Instr.	Filter	Exposure (s)	Pixel Scale ''	Seeing ''	Airmass
2007 Sep 05.25	Gemini-S+GMOS	g'	10×200	0.146	0.71	1.003
2007 Sep 11.09	Gemini-S+GMOS	r'	15×300	0.146	1.06	1.319
2007 Sep 05.29	Gemini-S+GMOS	i'	15×200	0.146	0.72	1.065
2011 Sep 21.21	Gemini-S+GMOS	g'	11×200	0.146	0.58	1.009
2011 Sep 21.26	Gemini-S+GMOS	r'	10×300	0.146	0.60	1.055
2011 Sep 24.15	Gemini-S+GMOS	i'	10×300	0.146	0.41	1.024
2001 Sep 16.00	VLT+FORs1	B_{BESS}	300	0.200	1.16	1.725
2001 Sep 16.00	VLT+FORs1	V_{BESS}	300	0.200	1.08	1.674
2001 Sep 16.00	VLT+FORs1	I_{BESS}	480	0.200	0.92	1.626
2011 Aug 18.24	VLT+FORs	B_{BESS}	3×480	0.252	0.58	1.036
2011 Aug 21.26	VLT+FORs	V_{BESS}	3×300	0.252	0.73	1.017
2011 Aug 18.23	VLT+FORs	I_{BESS}	5×200	0.252	0.55	1.061
2007 Oct 16.13	VLT+HAWKI	Y	6×60	0.106	0.81	1.010
2007 Oct 16.10	VLT+HAWKI	H	2×60	0.106	0.77	1.021
2011 Sep 16.22	VLT+HAWKI	Y	5×30	0.106	0.34	1.015
2011 Sep 16.30	VLT+HAWKI	H	5×10	0.106	0.36	1.153
2005 Oct 16.20	VLT+ISAAC	J	17×60	0.148	0.50	1.352
2005 Oct 16.10	VLT+ISAAC	K_S	58×60	0.148	0.37	1.112
2011 Sep 15.24	VLT+ISAAC	J	18×30	0.148	0.53	1.018
2011 Sep 15.24	VLT+ISAAC	K_S	18×15	0.148	0.44	1.029
2008 May 19.35	VLT+NACO	K_S	20×69	0.027	0.1	1.820
2011 Apr 29.99	HST+UVIS2	$F814W$	915	0.025
2011 Apr 29.99	HST+IR	$F125W$	828.577	0.078
2011 Apr 30.00	HST+IR	$F160W$	461.837	0.078

in Table 2, while photometry of the late-time HST observations is presented in Table 3. In comparing the pre-explosion and late-time observations (and the corresponding difference images), particularly in the IR, the object detected in the pre-explosion images is clearly no longer present; confirming the original identification of this star as the progenitor of SN 2008bk.

3.1 VLT FORs B,V & I

Our reanalysis of the pre-explosion *FORs BV* frames, in which the SN position was identified with a precision of $0.077''$, confirms the conclusion of Mattila et al. (2008): no single point source was present at the SN position. The new brightness limits determined for the pre-explosion *BV* images, having been calibrated against the corresponding photometry of the late-time images, are brighter than derived by Mattila et al. (which were inconsistent the brighter $\sim V$ magnitude calculated by Van Dyk et al. (2012) from the pre-explosion GMOS images). Our brightness limits, calculated using artificial star tests, take into account nearby sources in trying to recover a single point source at the SN position and, hence, we believe the brightness limits derived in this fashion are more reliable.

The bright positive residual in the *FORs BV* difference images (see Fig. 1), corresponding to an increase in brightness between the pre-explosion and late-time observation, appears much more diffuse than nearby point source residuals. The photometry of the source in the late-time *BV* images yields sharpness values of 0.7

and 1.1 respectively, implying that the SN residual has a broader and flatter profile than point sources.

The position of the SN on the pre-explosion *FORs I*-band image was identified to within $0.05''$, and we identify the same source found by Mattila et al. (2008) as the progenitor. The PSF-fitting photometry yields values similar to those found by Mattila et al., with $\chi^2 = 0.8$ and sharpness of 0.2 (consistent with a point source). Inspection of the late-time images clearly shows a large flux deficit at the SN position in the *I*-band image, although there is still a faint source coincident with the SN position (estimated to within $0.03''$). As for the pre-explosion images, the PSF-fitting photometry yields values consistent with a point source ($\chi^2 = 1.4$, sharpness = -0.1), unlike the residuals in the late-time *BV* images. Mattila et al. observed a bright source to the South of the SN position in the pre-explosion *ISAAC K_S*-band images, and we find a source at the same offset and position angle in the late-time *I*-band image (see section 3.4). The flux deficit between the pre-explosion and late-time *I*-band observations is clearly evident in the difference image (Fig. 1), and analysis of the residual is consistent with a point source. The source recovered in the late-time ground-based *I*-band image was found, in the corresponding HST observations (see section 3.4), to have a contributions from the fading SN; requiring an additional correction to the photometry derived from the difference images. The derived brightness for the progenitor (including the correction for late-time SN flux) is significantly lower than

the brightness determined from the pre-explosion images alone, but similar to the I -band brightness measured by Mattila et al..

3.2 Gemini GMOS-S g' , r' & i'

Van Dyk et al. (2012) reported the detection of a point source at the SN position in pre-explosion Gemini $g'r'$ images. In conjunction with the post-explosion NACO K_S image, we identify the same source in the pre-explosion GMOS $g'r'$ images, with an uncertainty of $0.05''$. Fitting the PSF to the pre-explosion source yielded $\chi^2 \sim 1$ while the sharpness parameter values, 0.50 and 0.68 for g' and r' respectively, are suggestive that the object is slightly extended; possibly due to the extended wings from the source to the North-West of the SN position (see Fig. 2). The photometry of this source in the GMOS images is approximately consistent with the upper limits placed on the source brightness in the pre-explosion *VLT FORS* images. Significant flux is still recovered at the SN position in the late-time g' and r' images, that is both brighter and more extended than the pre-explosion source and, similarly to the late-time *FORS BV* images, has a flatter, more extended profile. As the SN is still significantly brighter than the progenitor candidate (or detection limits thereon), image subtraction techniques cannot be used to probe the nature of the progenitor itself.

It is clear from Figs. 1 and 2, that there is additional extended flux around the SN position in the late-time images that was not present in the pre-explosion images. In the late-time Gemini GMOS $g'r'$ images, the apparent extended nature of the residual is clearer, especially in the r' -band difference image (where the effect of $H\alpha$ emission, either from the recombination in the local environment or from a light echo, is expected to be large - see section 3.4). The shapes of the pre-explosion source in the $g'r'$ images may suggest that crowding with nearby objects may cause the measured brightness of the progenitor in these two filters to be, possibly, overestimated (see below).

The SN position was identified to within $0.04''$ and $0.03''$ on the pre-explosion and late-time i' images, respectively. In both pre-explosion and late-time i' images, we recover a source at the SN position, whose properties are consistent with a point source. In the corresponding difference image, we see a negative residual due to the large flux deficit at the SN position between the two epochs. We also observe that the object immediately to the East of the SN progenitor has increased in brightness. As for the I -band observation, we apply a small correction to the i' brightness derived from the difference image, due to residual SN flux in the late-time image, derived from the late-time HST observations (see section 3.4).

We find the i' brightness of the progenitor, derived using image subtraction techniques, to be significantly less than determined by direct photometry on the pre-explosion images alone. This suggests that, although the pre-explosion i' photometry is dominated by the progenitor flux, it is blended with contributions from surrounding stars (as was also observed for the I -band observations). This may imply that a similar effect may apply to the photometry of the pre-explosion g' and r' observations. While the i' photometry is corrected for any contribution from blended flux, through template subtraction, the g' and r' observations are not and may, therefore, lead to an overestimate of the progenitor brightness. The additional uncertainties associated with the photometric zeropoints for the late-time g' and r' observations suggests that these two photometric measurements of the progenitor should be treated with some caution.

3.3 VLT HAWK-I/ISAAC Y, J, H & K_S

The VLT ISAAC J and K_S and HAWKI H images were common to the studies presented by Mattila et al. (2008) and Van Dyk et al. (2012). A pre-explosion Y -band observation was available in the archive, however it could not be photometrically calibrated in the original studies. The SN position was identified on the late-time $YJHK_S$ frames to within 0.016 , 0.052 , 0.024 and $0.037''$, respectively. A bright source is detected in all the pre-explosion $YJHK_S$ images at the SN position. The source appears consistent with a single point source in the JHK_S frames. PSF fitting to the source recovered in the Y frame yields $\chi^2 = 3.8$, suggesting it is possibly an extended source; however this may also be due to the poorer quality of the data compared to the JHK_S images. A source is subsequently recovered at the SN position in the late-time Y band image, although significantly fainter than the pre-explosion source. The SN is not detected as a point source in the late-time JHK_S images, to levels significantly fainter than the pre-explosion source; however, we note that there is diffuse emission at and around the SN position (and this is discussed in Section 3.4). Mattila et al. (2008) measured the PSF of the pre-explosion K_S source as being extended, hypothesising the pre-explosion source was a blend with a source located $\sim 0.5''$ South of the SN position. This source is recovered in the late-time K_S images.

The differences between the pre-explosion and late-time near-infrared images show significant residuals at the SN position consistent with the disappearance of the source detected in the pre-explosion images. In all cases, the corresponding residual is consistent with a point source. For the Y and J band observations, we find that the progenitor brightness determined using image subtraction techniques is fainter than estimated from the pre-explosion images alone. As for the I and i' observations, the difference suggests that blended flux from other sources contaminates the pre-explosion source. A small correction derived from the late-time HST observations was used to correct the progenitor's brightness determined from the Y and J difference images for possible residual SN flux. The K_S brightness derived from the difference image is slightly fainter than measured from the pre-explosion images, and may suggest contamination from the source to the South was not properly accounted for in photometry of the pre-explosion frame. The H -band photometry of the progenitor is identical for photometry of the pre-explosion images and from the corresponding difference image. In the ISAAC difference images (J and K_S), additional residuals are also seen for some nearby stars. The peculiar nature of these residuals, compared to the progenitor, suggests a possible deficiency with the calculated convolution kernel used to match the PSFs of the pre-explosion and late-time images. We note, however, that the scale of these residuals is small and that photometry of these residuals averages to zero brightness.

3.4 HST WFC3 $F814W$, $F125W$ & $F160W$

The late-time HST $F814W$, $F125W$ and $F160W$ observations of the site of SN 2008bk are presented on Figure 4. Photometry of the sources recovered at and around the SN position is reported in Table 3. In addition photometry was also conducted on late-time WFC3 UVIS $F336W$, $F555W$ and $F814W$ observations acquired as part of program GO-12285 (PI Soria) on 2011 May 07. Photometry of

these images was conducted using the `DOLPHOT` package⁵ (Dolphin 2000).

The SN is still recovered in all the images and, as reported by Van Dyk (2013), there is evidence for a light echo around the SN position. There are a number of sources around the SN (labeled in Figure 4) which are bright in the IR. The brightest nearby IR source is labeled Source E, which is the same source identified to the South of the SN position in the pre-explosion and late-time images. The diffuse emission recovered in the late-time ground based IR images (see Fig. 3 and Section 3.3) is shown to be a blend of SN emission, contributions from nearby stars and possibly the light echo. At redder wavelengths, the "diffuse emission" observed in the ground-based images clearly arises from the surrounding stars. Only one source in the vicinity of SN 2008bk is observed to have a blue SED (source G), however it is not as bright as the pre-explosion source recovered at the SN position in the ground-based pre-explosion optical images. We note, however, that the background at the SN position in the *F336W* and *F555W* is uneven and the wings of the bright blue sources to the North-West may have contributed to the flux measured in the pre-explosion Gemini GMOS-S *g'* and *r'* images. Although there are a number of IR sources around the SN position, these are significantly fainter than pre-explosion photometry of the progenitor (see Table 3). Since the IR brightness of the progenitor is derived from the difference images, these surrounding stars do not contaminate the progenitor photometry when derived in this manner.

As the SN is still recovered in the late-time HST observations, the photometry recovered from ground based images with late-time image subtraction must be corrected for the small amount of residual flux remaining at the SN position. We evaluated the corrections from the *F814W* and *F125W* images to be $\Delta I \approx \Delta I' = -0.1$ and $\Delta J = -0.025$; although we do not have a late-time HST observations corresponding to the ground-based *Y* filter, given the colour of the SN and the progenitor we interpolate between the corrections and estimate $\Delta Y \approx -0.05 - -0.08$. We note that these corrections are consistent with the differences between the pre-explosion and difference image photometry.

4 ANALYSIS

4.1 Distance, Metallicity & Reddening

Since the explosion of SN 2008bk, there have been two new recent distance measurements for the host galaxy determined using the tip of the red giant branch (T-RGB; Jacobs et al. 2009) and Cepheids (Pietrzyński et al. 2010), yielding $\mu = 27.79 \pm 0.08$ and 27.68 ± 0.09 mag, respectively. Given the agreement between the two most recent measurements, we adopt the mean for this study $\mu = 27.74 \pm 0.06$, corresponding to 3.5 ± 0.1 Mpc. The analysis of the progenitor of SN 2008bk presented by Mattila et al. (2008) utilised a larger distance $\mu = 27.96 \pm 0.24$ (Karachentsev et al. 2003), also derived from the TRGB, while Van Dyk et al. (2012) adopted the recent Cepheid distance above (although just using the systematic uncertainty); this gives rise to differences in distance modulus of $\Delta\mu = -0.22$ and $\Delta\mu = 0.06$ between our study and those of Mattila et al. (2008) and Van Dyk et al. (2012), respectively.

We recalculated the deprojected offset of the SN from the centre of the host galaxy, as previously determined in Mattila et al.

(2008). We find a smaller distance $r/R_{25} = 0.24$. This has consequences for the estimated metallicity at the SN position. The analysis of Mattila et al. (2008) assumed an LMC metallicity. Using the relations of Pilyugin et al. (2004), we derive an oxygen abundance at the radius of SN 2008bk of $12 + \log\left(\frac{O}{H}\right) = 8.42 \pm 0.07$. Assuming solar and LMC metallicities corresponding to abundances of 8.65 and 8.35 (Hunter et al. 2007), this corresponds to $\log(Z/Z_{\odot}) = -0.23$, just higher than the LMC value. Using the abundances derived to 27 H II regions, Bibby & Crowther (2010) derived a similar oxygen abundance-radius relation using the Pettini & Pagel (2004) *O3N2* indicator, yielding a corresponding metallicity at the radius of SN 2008bk of 8.52 (with average uncertainty on the sample of measurements of ± 0.1 dex). Van Dyk et al. (2012) measured the oxygen abundance for two H II regions, offset from the SN position, to be 8.45 and 8.52. These values are suggestive that the metallicity appropriate for the progenitor of SN 2008bk is likely to be intermediate between the LMC and solar values.

The Galactic foreground reddening towards SN 2008bk is $E(B - V) = 0.017$ mag (Schlafly & Finkbeiner 2011). Bibby & Crowther (2010) measured the Balmer decrement for 29 H II regions in NGC 7793, finding $E(B - V) = 0.18 \pm 0.02$ mags. Mattila et al. (2008) used the line strengths reported by McCall et al. (1985) to determine a reddening to the H II region W13, located $1.5'$ from SN 2008bk, to be 0.45 mags. The different levels of reddening measured towards H II regions suggest the possible role of significant and quite variable internal extinction inside NGC 7793. Reddening estimates derived from SN 2008bk are also conflicted. Van Dyk et al. (2012) suggested the absence of Na I D in the early photospheric spectrum of SN 2008bk, and its photometric similarity to SN 1999br, are indicative of negligible host reddening; whereas Morrell & Stritzinger (2008) claimed SN 2008bk was similar SN 1999em, which was subject to $E(B - V) \sim 0.1$ (Baron et al. 2000; Mattila et al. 2008).

4.2 Luminosity constraints for the progenitor from the K-band brightness

For standard values of R_V (e.g. 3.1), the effects of extinction are significantly reduced in the *K*-band compared to optical bands. The *K*-band magnitude derived for the progenitor of SN 2008bk, therefore, provides a reasonable constraint on the likely range of the luminosity of the progenitor. For MARCS model SEDs (the $5M_{\odot}$ spherical models with $\log g = 0.0$; Gustafsson et al. 2008), we considered the temperature range 2600 – 5000K (at approximately LMC and solar metallicities). Over this temperature range the bolometric correction with respect to *K* only changes by 0.8 mags, while BC_V changes by ~ 5.5 mags. While the interpretation of the *K*-band magnitude does depend on the extinction and temperature, the effects of these parameters are relatively small. On Figure 5 we show luminosity contours, over the full temperature range and reddenings in the range $0 \leq E(B - V) \leq 2$, given the *K*-band brightness measured for the progenitor from the difference imaging. From the *K*-band brightness alone, the luminosity of the progenitor is constrained to lie in the range $4.3 \leq \log(L/L_{\odot}) \leq 5.1$. Using the end point luminosities from STARS stellar evolution models for an LMC metallicity (Smartt et al. 2009), this limits the progenitor to having an initial mass $< 15 - 17M_{\odot}$.

4.3 SED fitting

We considered the observed photometry, and upper limits, with respect to SEDs derived from MARCS synthetic spectra (Gustafsson

⁵ <http://americano.dolphinim.com/dolphot/>

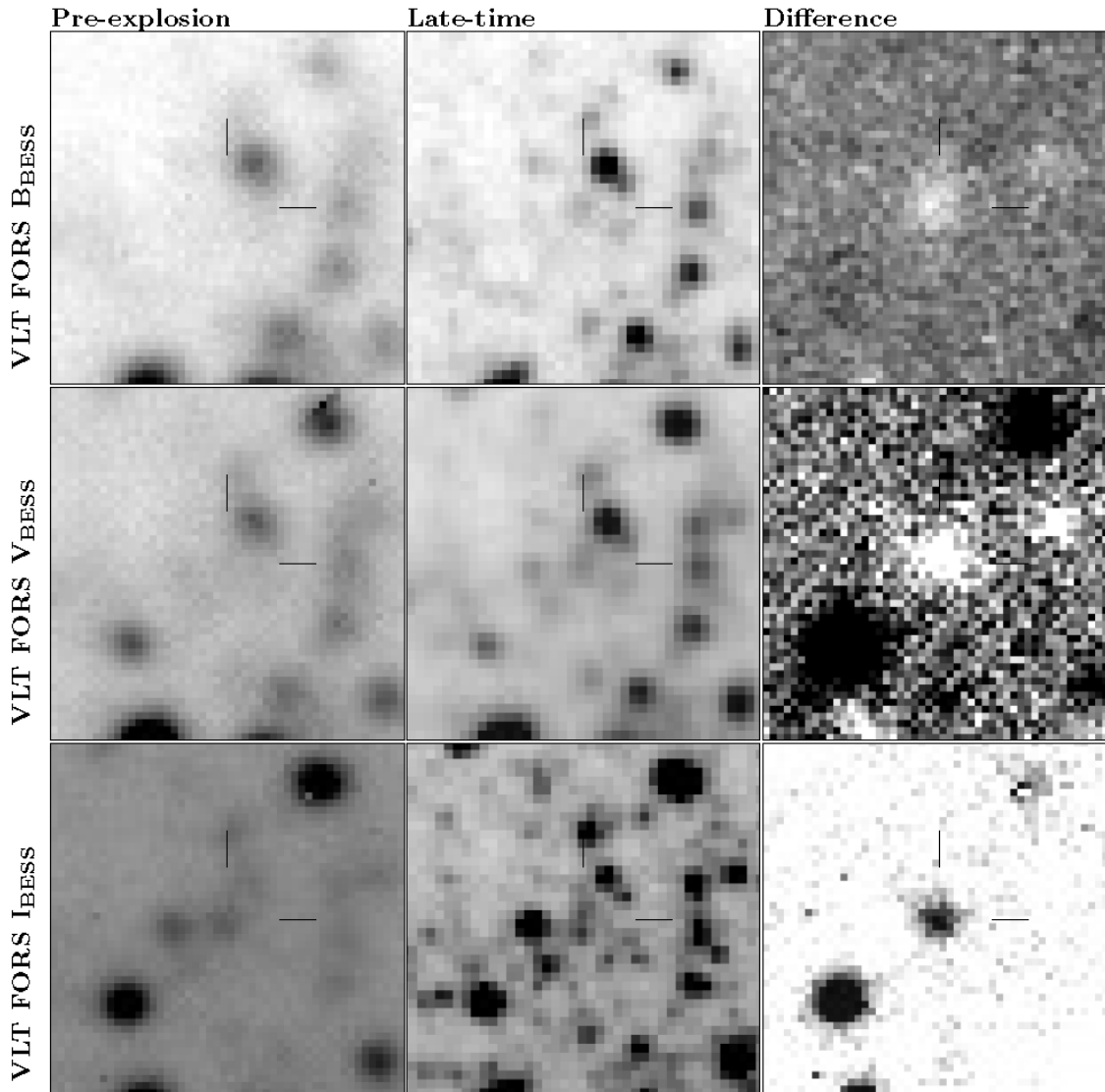


Figure 1. Pre-explosion and late-time VLT FORS images of the site of SN 2008bk, in the B , V and I filters. The difference image, between the pre-explosion and late-time frames, is shown in the righthand column. The images have dimensions $10'' \times 10''$ and are oriented such that North is up, East is left. The position of SN 2008bk, in all the images, is indicated by the cross hairs. In the difference images positive (lighter) residuals correspond to source brighter in the late-time images, while negative (darker) residuals correspond to sources that are fainter in the late-time images. Details of these observations are presented in Table 1.

et al. 2008). The SEDs fits were conducted using our own Bayesian SED fitter (Maund, 2013, in prep), which allow us to probe the effects of different metallicities and reddening laws on the interpretation of the observations.

We considered the $5M_{\odot}$ spherical MARCS models with surface gravity $\log g = 0$ and metallicities equivalent to $\log(Z/Z_{\odot}) = -0.25$ (“LMC”) and solar metallicity ($\log(Z/Z_{\odot}) = 0.0$). In order to probe different types of dust in the ISM in the host galaxy we computed synthetic photometry for reddening laws with $R_V = 2, 3.1, 4$ and 5 (Cardelli et al. 1989). We also considered synthetic photometry for a mixture of dust components, with foreground Galactic reddening $0 \leq E(B - V) \leq 0.2$ (consistent with the reddening estimated by Van Dyk et al. (2012)) and a Silicate dust component with $0 \leq \tau \leq 20$ (Kochanek et al. 2012).

To assess the sensitivity of the fits to particular data points

(specifically the uncertain g' and Y photometry) we considered four groups of the photometric measurements containing all or subsets of the data. Each dataset is composed N photometric measurements and M upper limits. Our Bayesian SED fitter, based on the Nested Sampling algorithm (Skilling 2004), calculates the Bayesian evidence (the marginal likelihood) as a measure of the relative quality of the fits to different models to the same dataset. For each dataset, we consider the relative Bayesian evidence for each model (i.e. the Bayes factor) with respect to the model with LMC metallicity and $R_V = 3.1$. We report Bayes factors (K ; in decibans) and, in this instance, χ^2 values. In the general case of considering datasets containing upper limits, the meaning of χ^2 and the corresponding p -values depart from their normal definitions. The upper limits provided by the pre-explosion FORS BV photometry are not constraining and do not, in this case, impact the definition of the χ^2 p -value. The outcome of the SED fits are reported in Table 4.

Before considering the problem of parameter estimation, it is

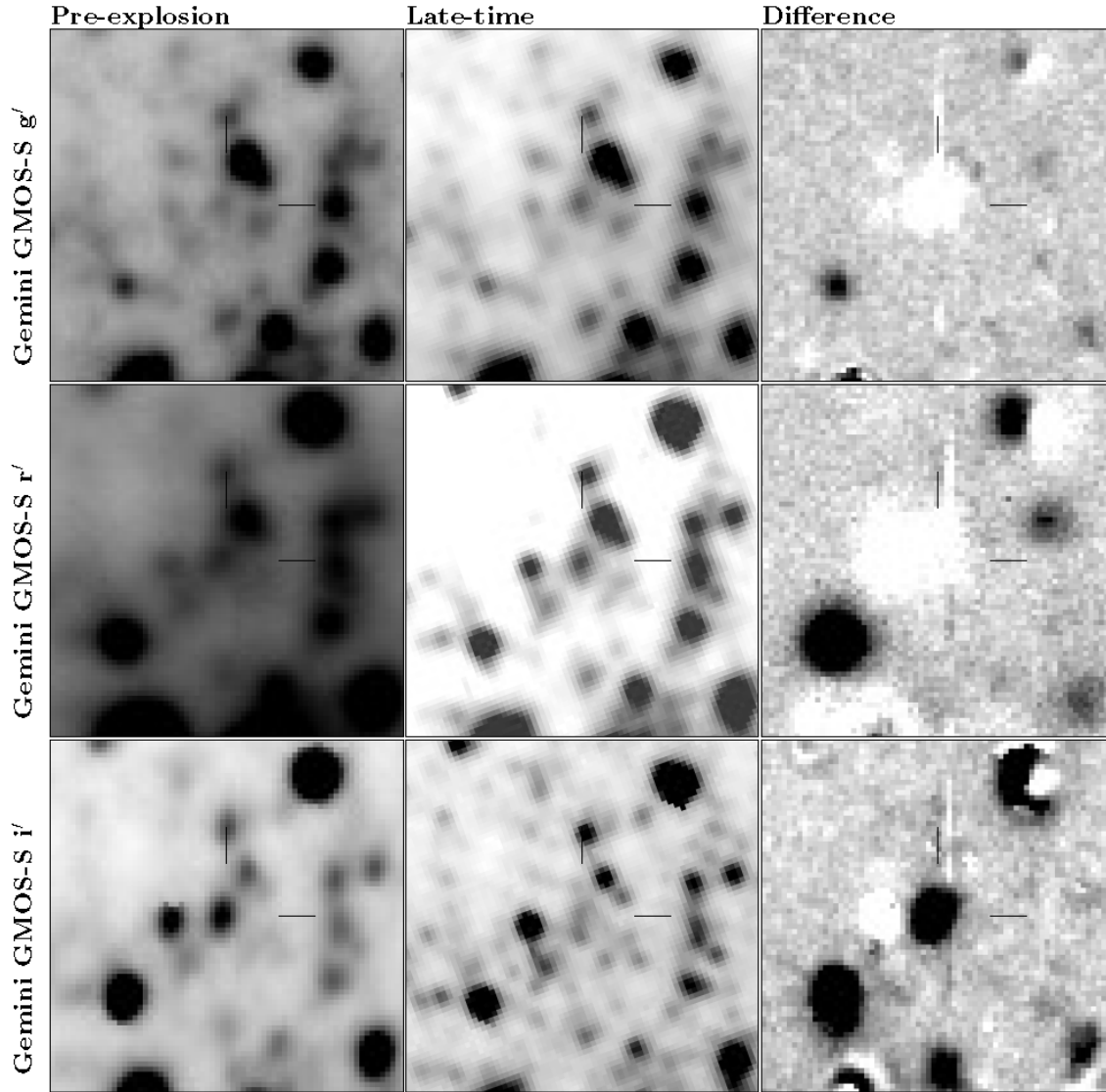


Figure 2. Pre-explosion and late-time Gemini GMOS-S imaging of the site of SN 2008bk, in the g' , r' and i' filters. For a description of the columns, see Figure 1.

Table 2. Pre-explosion, late-time and difference image photometry of the site of SN 2008bk

Band	Pre-explosion	Late-time	Difference	Progenitor	Mattila et al.	Van Dyk et al.
B	> 22.77(0.17)	23.12(0.13)	...	> 22.77(0.17)	> 22.9	
V	> 22.19(0.05)	21.97(0.08)	...	> 22.19(0.05)	> 23.0	22.81(0.09)
I	20.81(0.04)	22.99(0.14)	21.36(0.05)	21.26(0.06) [†]	21.20(0.19)	20.71(0.08)
g'	23.96(0.10)	22.65(0.04)	...	23.56(0.04)
r'	22.47(0.07)	22.34(0.05)	...	22.27(0.02)	...	22.03(0.07) [‡]
i'	20.89(0.01)	23.06(0.07)	21.42(0.06)	21.32(0.06) [†]
Y	19.88(0.11)	22.69(0.11)	20.13(0.18)	20.05(0.17) [†]
J	19.34(0.02)	> 22.67(0.10)	19.47(0.03)	19.47(0.03)	19.50(0.06)	19.26(0.14)
H	18.54(0.04)	> 20.08(0.06)	18.52(0.04)	18.52(0.04)	18.78(0.11)	18.55(0.06)
K_S	18.31(0.03)	> 20.13(0.12)	18.39(0.03)	18.39(0.03)	18.34(0.07)	18.14(0.10)

[†] Progenitor magnitude is a combination of the pre-explosion/late-time brightness difference and the late-time brightness.

[‡] R -band photometric measurements derived from an underlying r' observation.

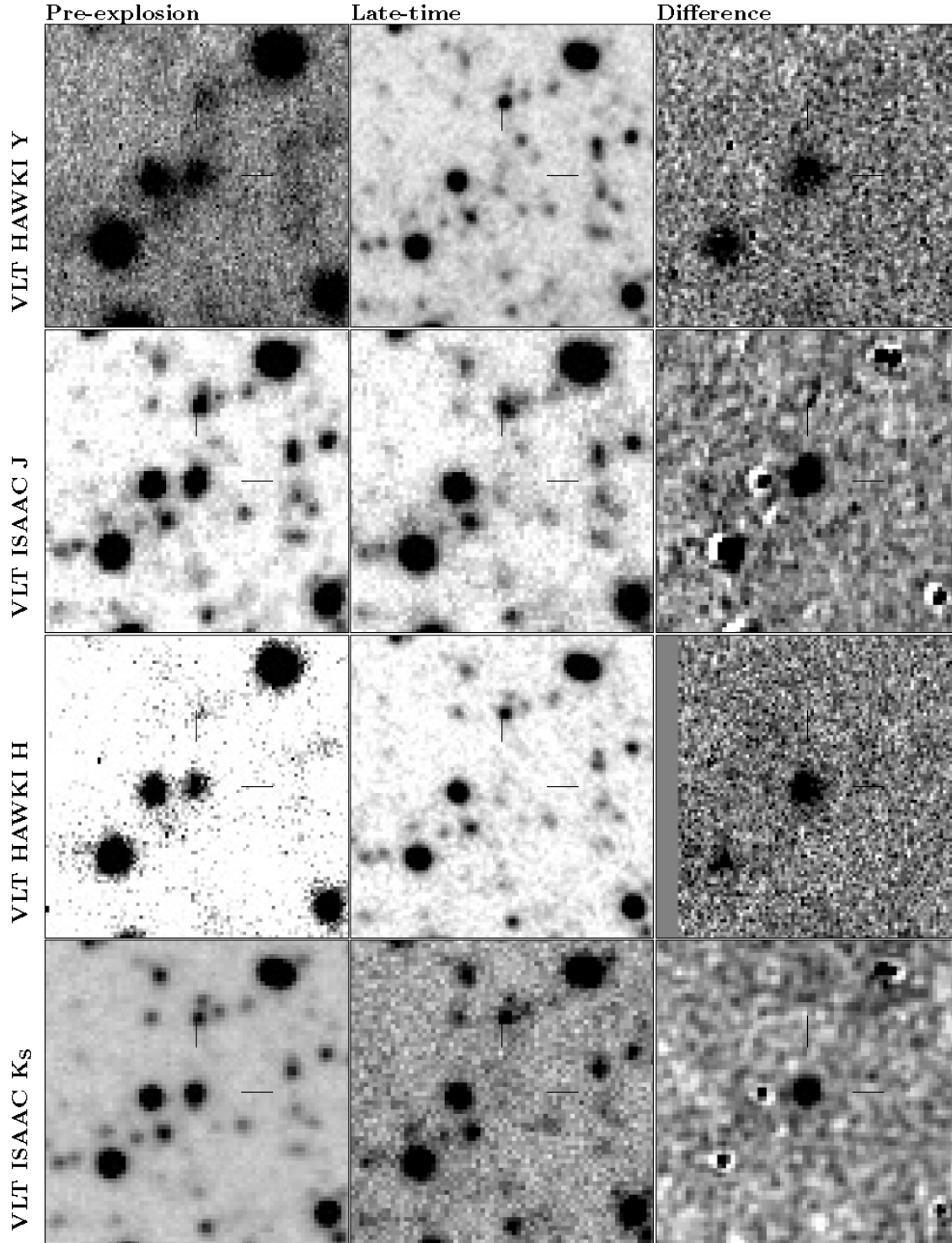


Figure 3. Pre-explosion and late-time VLT Near-Infrared HAWKI-I and ISAAC imaging of the site of SN 2008bk, in the Y , J , H and K_S filters. For a description of the columns, see Figure 1.

clear from Table 4 that, in general, the solar metallicity models provide a slightly worse fit to the observational data (regardless of the choice of the underlying dataset) but not at a greatly significant level. Table 4 also highlights the role of the g' photometric point. Those datasets containing the g' measurement provide a significantly worse χ^2 than datasets without and also favour reddening laws with higher R_V . We note that large values for χ^2 achieved

for datasets containing g' are principally due to the MARCS models under-predicting the flux, relative to the observed value, at that wavelength. Conversely, the inclusion of the Y -band photometric point has little impact on the quality of resulting fits. For datasets in which the g' point is not included, we see that there is little evidence for achieving better fits with higher R_V (although the low value of

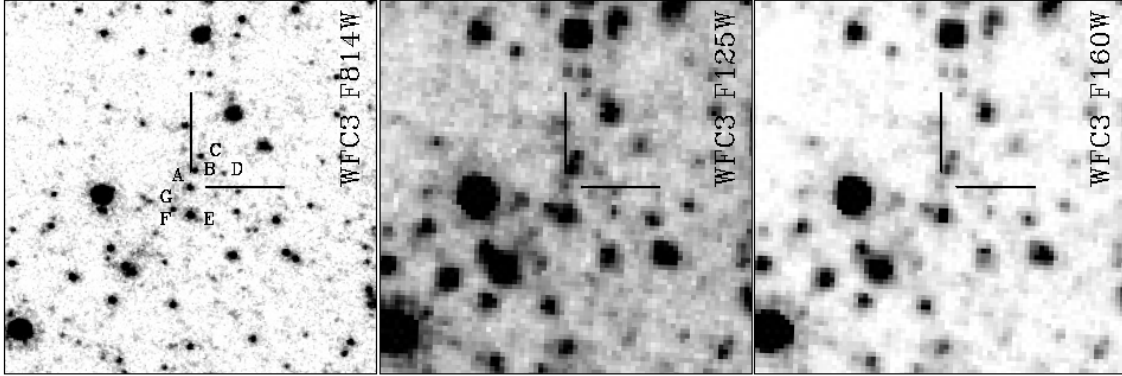


Figure 4. Late-time HST WFC3 UVIS and IR channel imaging of the site of SN 2008bk, with the $F814W$, $F125W$ and $F160W$ filters. The images are centred of the SN position, indicated by the cross hairs (labeled A), and oriented such that North is up, East is left. Each of the frames has dimensions $6'' \times 6''$. The SN and surrounding stars are labeled A – G (see text).

Table 3. Late-time HST photometry of SN 2008bk and surrounding stars

	2011 May 07			2011 Apr 29		
	$F336W$	$F555W$	$F814W$	$F814W$	$F125W$	$F160W$
A(SN)	23.57 ± 0.05	24.14 ± 0.02	24.01 ± 0.04	23.84 ± 0.05	24.50 ± 0.07	23.95 ± 0.23
B	...	26.36 ± 0.08	24.16 ± 0.04	24.06 ± 0.05	22.63 ± 0.05	22.19 ± 0.06
C	...	26.49 ± 0.09	24.28 ± 0.04	24.21 ± 0.05	22.85 ± 0.06	22.55 ± 0.06
D	...	26.57 ± 0.10	24.89 ± 0.07	24.86 ± 0.06	23.74 ± 0.08	23.16 ± 0.08
E	...	25.28 ± 0.04	23.10 ± 0.02	23.00 ± 0.04	21.82 ± 0.06	21.48 ± 0.13
F	...	26.01 ± 0.07	24.24 ± 0.04	24.22 ± 0.06	22.84 ± 0.08	22.31 ± 0.12
G	24.20 ± 0.07	25.35 ± 0.04	25.50 ± 0.17	25.36 ± 0.10

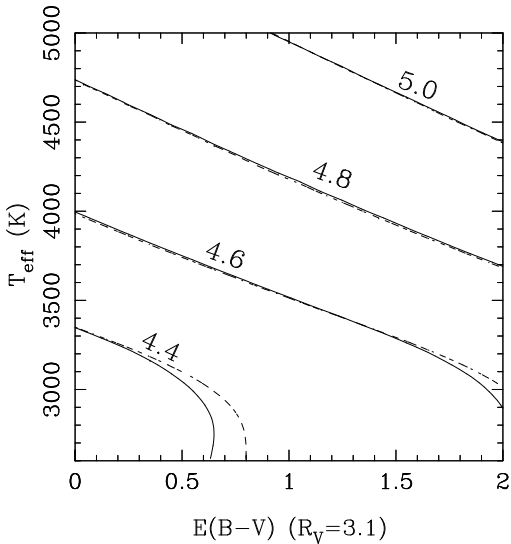


Figure 5. Constraints on the luminosity of the progenitor of SN 2008bk from the observed K -band brightness (under the assumption of a $R_V = 3.1$ reddening law). The solid and dashed contours corresponds metallicities of $\log(Z/Z_\odot) = -0.25$ and 0.0 , respectively.

$R_V = 2$ provides a generally worse fit). The dust mixture model (with ISM and Silicate dust composition) is also disfavoured.

The observed photometry could also be compared with MARCS models with different stellar mass, in particular the spherical $15M_\odot$ models. At the time of writing these models are only

available for $\log g = 0.0$ at solar metallicity, and cover a smaller temperature range ($3300 - 4500K$). We have compared the synthetic photometry of the 5 and $15M_\odot$ solar metallicity models and find that the differences in predicted colours predominantly affect bluer colours and are generally small and reddening independent. The largest difference is for the $g' - r'$, corresponding to an absolute colour difference of only 0.06 mags at $3300K$, while at near infrared wavelengths the colour differences are negligible. We do find that the Johnson $B - V$ colour does show some sensitivity to reddening, again at the coolest extreme of the temperature range, but only ~ 0.04 mags. We have applied the same fits with the solar metallicity $15M_\odot$ to the observed datasets and find that the differences in quality of the fits is small when compared to, for example, the effect of metallicity; so we do not consider the $15M_\odot$ models further.

To explore the parameters of the progenitor we consider the dataset composed of all the photometric detections and non-detections except the Gemini GMOS g' observation. Posterior samples, generated during the determination of the Bayesian evidence for the SED fitting process, were used to estimate the median and 68% probability interval for each of the model fits to the observed SED of the progenitor. The best fit parameters, for different assumptions of metallicity and reddening law, are presented in Table 5. As expected, increases in the value of R_V yield lower reddenings and higher temperatures for the progenitor. For each reddening law, the assumption of solar metallicity results in a slightly hotter, less reddened progenitor. The inclusion of a Silicate dust component, under the assumption of low interstellar reddening (see above),

Table 4. The results of SED fits to MARCS synthetic spectra to the observations of the progenitor of SN 2008bk.

log(Z/Z_{\odot})		$R_V = 2$	$R_V = 3.1$	$R_V = 4$	$R_V = 5$	$R_V = 3.1 + \text{Sil}$
$g'r'i'BVIYJHK_S$ ($N = 8, M = 2$)						
-0.25	K	-29.4 ± 0.4	0.0 ± 0.0	14.2 ± 0.4	21.0 ± 0.4	-33.3 ± 0.6
	χ^2	36.0	22.0	15.2	10.6	31.47
0.0	K	-33.5 ± 0.4	-4.2 ± 0.4	9.7 ± 0.4	16.8 ± 0.4	-39.8 ± 0.6
	χ^2	38.1	23.9	17	12.3	34.0
$g'r'i'BVIJHK_S$ ($N = 7, M = 2$)						
-0.25	K	-29.2 ± 0.4	0.0 ± 0.0	13.4 ± 0.4	19.8 ± 0.4	-33.5 ± 0.4
	χ^2	35.5	21.7	15	10.2	30.7
0.0	K	-34.0 ± 0.4	-4.6 ± 0.4	8.9 ± 0.4	16.6 ± 0.4	-37.7 ± 0.4
	χ^2	37.7	23.7	16.8	12	33.4
$r'i'BVIJHK_S$ ($N = 6, M = 2$)						
-0.25	K	-5.9 ± 0.4	0.0 ± 0.0	1.4 ± 0.4	-0.7 ± 0.4	-13.1 ± 0.5
	χ^2	8.7	5.4	5.3	5.6	8.3
0.0	K	-9.4 ± 0.4	-1.8 ± 0.4	-1.7 ± 0.4	-3.3 ± 0.4	-16.5 ± 0.5
	χ^2	10.1	6.9	6.8	6.7	10.0
$r'i'BVIYJHK_S$ ($N = 7, M = 2$)						
-0.25	K	-6.6 ± 0.4	0.0 ± 0.0	-1.0 ± 0.4	-2.1 ± 0.4	-14.6 ± 0.5
	χ^2	9.02	5.8	5.8	6.1	8.8
0.0	K	-9.9 ± 0.4	-2.6 ± 0.4	-3.2 ± 0.4	-11.6 ± 0.4	-17.1 ± 0.5
	χ^2	10.3	7.1	7.1	7.7	10.3

yields not only a poor solution (see Table 4) but also low values of τ .

For the LMC and solar metallicities, assuming $R_V = 3.1$, the best fit solution to the observed data (excluding the g' observation) is presented on Figure 6. From this analysis, the joint posterior distribution for the temperature and reddening of the progenitor (Figure 6a) shows the standard degeneracy, with SEDs with increasing temperatures requiring corresponding increases in reddening to match the observed colours of the progenitor object. The contours for the solar and LMC metallicities almost completely overlap, although there are some minor differences, and this is reflected in slight differences seen in Table 4 for model fits with different metallicities. The model SED (Figure 6b) provides a good match to the observations, although we note the H -band magnitude appears to lie above the 68% interval by 1σ . The model fits are dominated by the IR photometry and, hence, the best SED fits consistently underestimate the observed g' flux.

The luminosity and temperature constraints for the progenitor on the HR diagram (Figure 6c) show the degeneracy between the temperature and the derived bolometric luminosity (through the bolometric and extinction/reddening corrections). The luminosity-temperature contours only slightly overlap the model points for the end of He-burning for a $13M_{\odot}$ star, but do not extend to cooler tem-

peratures consistent with the actual end points of the STARS stellar evolution models (Eldridge & Tout 2004), at which core-collapse is expected to take place. The slope of the contours lies approximately parallel to the direction of constant radius of the HRD, with the progenitor's radius constrained to $\sim 400-500R_{\odot}$ for both the LMC and solar metallicity models. The luminosity derived from the SED fitting analysis is consistent with the luminosity constraints derived from the K_S -band brightness.

We adopt the same technique presented by Maund et al. (2013) to determine the mass probability density function for the LMC and solar metallicity SED fits with $R_V = 3.1$. Maund et al. assume that, for a given luminosity, the progenitor has a uniform probability of having a mass between the maximum mass for a star to end He-burning at that luminosity and the minimum mass for a star to terminate (i.e. the final end point of the model) at that luminosity. Using the luminosity probability distributions derived above, in comparison with the He-burning and model end points presented by Smartt et al. (2009), we derive the probability density function for the progenitor having a specific initial mass (see Figure 6d). The mass estimates for the two metallicities considered are similar, although the solar metallicity yields a slightly higher mass. For $R_V = 3.1$, we derive $M_{init} = 12.9^{+1.6}_{-1.8}M_{\odot}$ and $13.8^{+1.6}_{-1.8}M_{\odot}$ for LMC and solar metallicities respectively.

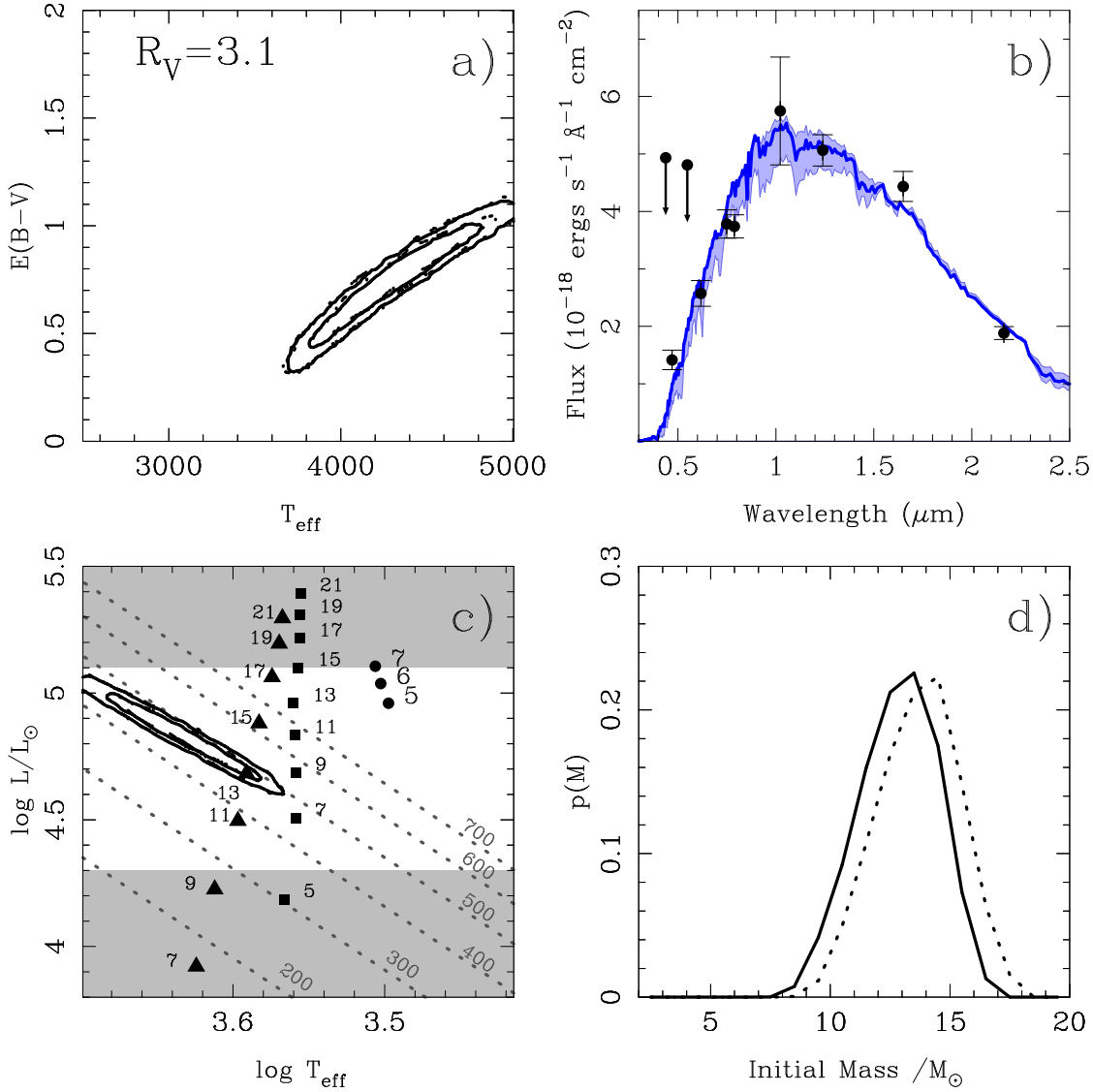


Figure 6. The derived properties of the progenitor of SN 2008bk, assuming $R_V = 3.1$ for $\log(Z/Z_\odot) = -0.25$ and 0.0 . *a*) The joint posterior distribution for reddening $E(B - V)$ and temperature T_{eff} . The solid and dashed contours correspond to metallicities of $\log(Z/Z_\odot) = -0.25$ and 0.0 , respectively. The contours contain 68% and 95% of the probability for each model fit. *b*) The observed photometry, and detection limits, of the progenitor compared to the best fit SED model (heavy blue line). The light blue shaded region are the SED boundaries corresponding to the 68% probability interval. *c*) The position of the progenitor on the HR diagram. The meaning of the contours is the same as above. The shaded regions indicate locations on the HR diagram that are inconsistent with the measured K_S -band brightness. Over-plotted are the points from LMC metallicity STARS stellar evolution models, with initial masses as labeled, corresponding to the positions of the end of He-burning (\blacktriangle), the termination point of the models (\blacksquare) and the termination point for those stars that become SAGB stars (\bullet). The dashed grey lines show lines of constant radius on the HR diagram. *d*) Mass probability density distributions for the progenitor of SN 2008bk, for $\log(Z/Z_\odot) = -0.25$ (solid) and 0.0 (dashed).

5 DISCUSSION & CONCLUSIONS

5.1 The nature of the progenitor of SN 2008bk

We have measured the properties of the progenitor of Type IIP SN 2008bk in pre-explosion observations coupled with late-time observations, using the same telescopes and instruments, in which the progenitor (and the SN) are no longer observed. The absence of the pre-explosion star in the late-time images confirms the original identification of this star as the progenitor (Mattila et al. 2010). Using image subtraction techniques we have determined the infrared brightness of the progenitor to much higher precision than allowed by using the pre-explosion observations alone. With the benefit

of late-time *HST* observations we have estimated the residual SN flux contamination to our template subtraction analysis, as well as demonstrated that there is little contamination at IR wavelengths from surrounding stars. In the optical, the complex and crowded nature of the region hosting the SN most probably leads to over-estimates of the progenitor brightness from photometry of the pre-explosion observations alone. With the revised SED, constructed from improved photometry, we have shown the progenitor has a relatively high mass for a Type IIP SN progenitor: $\sim 13M_\odot$. The progenitor is found to have suffered large reddening and, correspondingly, had a high temperature.

Our method for determining the masses of the progenitors

Table 5. The best fit parameters for the progenitor of SN 2008bk.

R_V	$\log(Z/Z_\odot)$	$E(B - V)$	$T_{eff} (K)$	$\log(L/L_\odot)$	R/R_\odot	M/M_\odot
2	-0.25	$0.98^{+0.22}_{-0.23}$	4025^{+215}_{-180}	4.71 ± 0.07	465 ± 14	11.3 ± 1.5
	0.0	1.00 ± 0.24	4030^{+235}_{-190}	4.72 ± 0.07	470^{+13}_{-16}	12.4 ± 1.7
3.1	-0.25	$0.77^{+0.17}_{-0.21}$	4330^{+330}_{-335}	4.84 ± 0.11	470 ± 16	$12.9^{+1.6}_{-1.8}$
	0.0	$0.78^{+0.17}_{-0.21}$	4325^{+340}_{-330}	4.85 ± 0.11	475 ± 16	$13.8^{+1.6}_{-1.8}$
4	-0.25	$0.63^{+0.12}_{-0.17}$	4450^{+350}_{-390}	4.88 ± 0.11	475 ± 16	$12.9^{+1.6}_{-1.8}$
	0.0	$0.64^{+0.13}_{-0.18}$	4475^{+360}_{-420}	$4.90^{+0.11}_{-0.14}$	475 ± 17	$15.5^{+1.7}_{-2.0}$
5	-0.25	$0.50^{+0.10}_{-0.15}$	4480^{+365}_{-415}	$4.91^{+0.12}_{-0.15}$	475 ± 14	$13.9^{+1.6}_{-2.2}$
	0.0	$0.57^{+0.05}_{-0.08}$	4775^{+170}_{-295}	$5.00^{+0.05}_{-0.09}$	465 ± 12	15.5 ± 1.4
3.1 + Sil	-0.25	$\tau = 3.3^{+0.8}_{-0.9} \dagger$	3890^{+150}_{-130}	4.65 ± 0.04	465 ± 15	10.5 ± 1.4
	0.0	$\tau = 3.3^{+0.8}_{-1.0} \dagger$	3880^{+160}_{-130}	4.65 ± 0.05	465 ± 16	11.7 ± 1.6

is different to those previously used, in particular the technique adopted by Smartt et al. (2009). We believe our methodology, presented by Maund et al. (2013), is more robust because it correctly couples the uncertainties on the observed luminosities with the uncertainty on what luminosity, between the end of core He-burning and the model end point, an RSG progenitor may actually be observed at. The consideration of the various parameters underlying the SED fits (such as a reddening law and metallicity), through the use of a complete family of SED models, means that we can comprehensively assess systematic effects. The improved precision of our progenitor photometry, in conjunction with the systematic comparison of the observations with model RSG SEDs, leads to a more precise and confident mass estimate for the progenitor of SN 2008bk than has been previously achieved for any other Type IIP SN from pre-explosion images. In section 5.2, we compare the results of this new analysis with the previous estimates of the progenitors properties for SN 2008bk.

As found previously by Maund et al. for other RSG progenitor detections, this new approach yields four interesting results concerning the progenitor of SN 2008bk: 1) the initial mass probability density function extends up to slightly higher masses than suggested by the previous analysis; 2) there is evidence for the presence of significant dust affecting the progenitor, that is not perhaps observed in post-explosion observations of the SN; 3) the effect of this dust is well described by a standard reddening law consistent with ISM dust; and 4) the derived temperature of the progenitor is higher than would be expected if the progenitor was a late M-supergiant.

5.2 Results from previous analyses

Previous analyses of the progenitor of SN 2008bk have been presented by Mattila et al. (2008), Van Dyk et al. (2012) and Davies et al. (2013). The analysis of Davies et al. is based on the photometric measurements presented by Mattila et al., while Van Dyk et al. present a reanalysis of the same IR data used by Mattila et al. supplemented with optical detections of the progenitor. In this paper, we have reanalysed all the previously presented pre-explosion datasets, with more accurate calibrations based on late-time observations of the same fields acquired under photometric conditions.

A comparison of the photometry derived here and those of the previous studies is presented in Table 2. The VLT IR photometry

common to both previous studies shows some agreement and disagreement with our photometry. The J and K_S magnitudes we measure from the ISAAC data are almost identical to those presented by Mattila et al., whilst being 0.2 – 0.3 mags fainter than measured by Van Dyk et al.. Conversely, our H -band measurement from the HAWKI data agrees with Van Dyk et al., but is 0.26 mags fainter than measured by Mattila et al..

The key measurements affecting the analysis of the SED are the Cousins I and Sloan i' brightnesses. We find our measurements of the I -band brightness to be almost identical to those of Mattila et al., although slightly fainter due to the removal of contaminating flux from surrounding stars through the use of template subtraction with late-time images. The measurement by Van Dyk et al. is significantly higher, however the full origin of this discrepancy is difficult to identify as they bootstrapped their i' photometry to Cousins I (see below); and the same is the case for comparing our g' and r' photometry with their VR photometry. Given the apparent consistency we achieve independently between our VLT FORS Cousins I and Gemini i' photometry, we believe that the lower value of the I band brightness is correct. Even though we have established the stability of observing under photometric conditions with Gemini GMOS, over the period in which the late-time observations were conducted, the lack of photometric standards observed on the same night as late-time g' and r' observations raises some concern about the size of the uncertainties estimated for these two measurements.

Using late-time HST observations we have established that the degree of contamination of the pre-explosion photometry from *unresolved* blended stars was smallest at optical wavelengths. At IR wavelengths the pre-explosion photometry of the source at the SN position is dominated by the bright progenitor, compared to other, fainter sources nearby (see Table 3). It is not surprising that, at IR wavelengths, the photometry of the progenitor in the pre-explosion images with and without late-time image template subtractions should be similar. As evident from the optical ground-based images, the region in which SN 2008bk is located is crowded, such that PSF photometry of a single object may be suboptimal in the presence of bright, yet resolved neighbours. We specifically note the discrepancy between our photometry of the pre-explosion i' source, from the pre-explosion image alone, and the final magnitude we derive for the progenitor with the benefit of template

subtraction. As our g' and r' photometry was not conducted with the benefit of template subtraction, due to the SN still being bright at these wavelengths, these measurements maybe be overestimates due to the effect of crowding (as shown by the i' photometry). This may partially explain the apparent discrepancy between the model SEDs and the g' photometry, and may cast doubt over the veracity of the r' measurement. The differences between our analysis and the previously published studies highlights the importance of acquiring late-time observations of SNe with identified progenitors: to not only confirm the disappearance of the progenitor, but to also achieve both precise and accurate photometry of the progenitor object.

Using the previously reported photometry of Mattila et al. and Van Dyk et al., we conducted the same analysis as presented in Section 4.3 on their datasets. The derived properties of the progenitor given these previous measurements are presented on Figure 7.

The reanalysis of the Mattila et al. data by Davies et al. (2013) is consistent with the result derived here with an expanded dataset. Davies et al. derive a mass of $12^{+2}_{-1}M_{\odot}$, higher than the mass derived by Mattila et al. using the same dataset. The two studies, however, used fundamentally different underlying SEDs to estimate the progenitor parameters. Like us, Davies et al. compared this observed photometry with MARCS SEDs, whereas Mattila et al. compared their photometry with the empirical RSG colour scheme of Elias et al. (1985). Our reanalysis of the Mattila et al. photometry, as published, and the similarity with the result obtained by Davies et al., might suggest the fundamental difference in the result is due to the differences in the choice of underlying SEDs; however, as discussed below, we do not believe this is the case. We note that the parameters of the progenitor, as constrained by the Mattila et al. dataset, do not completely resolve the degeneracy between temperature and reddening, as indicated by the barely closed contours on Figure 7, although they favour the high temperature solution found in our analysis.

In their original analysis, Mattila et al. favoured a low mass progenitor ($M_{\text{init}} = 8.5 \pm 1M_{\odot}$), assuming an M4 spectral type. They also noted, however, that the observed SED might also be accommodated with a progenitor with earlier spectral type and higher reddening (going so far as to consider a G-type yellow supergiant). For an M0 supergiant progenitor, with $T_{\text{eff}} = 3750K$ and $A_V = 3$, they suggested a mass as high as $11 \pm 2M_{\odot}$, which is approaching the value determined here (although with higher reddening).

As for the progenitor of SN 2012aw (Fraser et al. 2012), the Mattila et al. analysis was based on four photometric measurements. It is clear from our analysis of the progenitor of SN 2008bk, with the expanded dataset, that > 4 photometric points are required to adequately constrain the progenitor SED and break the degeneracies between temperature and reddening.

The analysis by Van Dyk et al. suggested a low reddening towards the progenitor, however our reanalysis, despite using the same synthetic spectra, suggests a different picture. It is evident from Figure 7, for their photometry, that the bulk of the probability in the reddening/temperature plane lies at negative reddening (driven by the g' measurement). The apparent need for negative reddening to provide an adequate fit to the theoretical SEDs may suggest: 1) the models are incompatible with the observed data or 2) the data are incompatible with the theoretical models (based on our photometry, we favour the latter). The low reddening quoted by Van Dyk et al. is in actuality a "grid edge" effect, based on the assumption that $E(B - V) \geq 0$. Such an assumption could be introduced into our analysis of their dataset, in the form of a prior, however we note that: 1) the corresponding Bayesian evidence would

be even lower than the value determined for the complete parameter space; and 2) the most probable solution would then be with high reddening and temperature. When including the negative reddening solution, the Van Dyk et al. dataset yield a bimodal solution; with the negative reddening solution supporting a low mass progenitor (consistent with their estimate of $8 - 8.5M_{\odot}$) and the other probability peak consistent with a high mass progenitor (at the extreme of the mass range determined by our analysis).

5.3 Implications for RSGs

The temperature inferred for the progenitor of SN 2008bk is higher than generally reported for RSGs. We have principally compared our observations with the Cambridge STARS code (Eldridge & Tout 2004), which generally predicts RSGs to have cooler temperatures. The inclusion of rotation into the models of Ekström et al. (2012), for $\log(Z/Z_{\odot}) \sim -0.15$, does not cause a significant change in the predicted temperatures of RSGs, when compared with their non-rotating models (at the luminosity at which we have observed the progenitor of SN 2008bk). Smartt et al. (2009) presented a compilation of the temperatures at the endpoints, for a range of initial masses, of a variety of different stellar evolution models (see their Fig. 3), which are all significantly cooler than the temperature we measure here.

Our inferred temperature agrees with the temperature-colour relation presented by Levesque et al. (2006), where for the progenitor of SN 2008bk we find $(V - K)_0 = 3.04$. Following the spectral type sequence of Levesque et al., the progenitor of SN 2008bk would be considered to have spectral type K1; significantly earlier than the canonical prediction of M-supergiants as the progenitors of Type IIP SNe, and just as hot as the progenitor of the Type IIB SN 1993J (Aldering et al. 1994; Maund et al. 2004).

An important concern, therefore, is that either the MARCS SEDs yield solutions that are too hot or stellar evolution models underestimate the temperature of the progenitors. We note, however, that the intrinsic colours for the progenitor (for the best fit solution) are also consistent with the colour sequence of Elias et al. (1985); and, following their spectral type sequence, we again find the progenitor is consistent with an early K-supergiant. While our result is dependent on MARCS SEDS, we note that Walmswell & Eldridge (2012) derived a similar mass but using the BaSeL standard stellar library (Westera et al. 2002, and references therein). Conversely, the temperatures predicted by stellar evolution models may be "tuned" through the assumptions of different opacities and mixing lengths.

Davies et al. (2013) recently compared temperature estimates for RSGs derived using SED fitting techniques (similar to those used here) and the strengths of the TiO bands. Davies et al. found that temperatures determined from the strength of the TiO bands are generally lower ($\sim 400 - 500K$) than those derived from IR photometry; and, furthermore, the strength of the TiO bands were observed to be correlated with the luminosity of the RSG. In light of the new analysis by Davies et al., we find that the temperature for the progenitor of SN 2008bk is not unusual. In previous analyses, with single detections or upper limits, we have had to assume the temperature/spectral type of a cool RSG (see e.g Smartt et al. 2009); such that if the temperatures were underestimated, the corresponding bolometric luminosities were overestimated (making the RSG problem even worse). Our recent reanalysis of the pre-explosion observations of the progenitors of SNe 2003gd and 2005cs have, similarly, resulted in hotter temperature constraints (in the similar

temperature range as the progenitor of SN 2008bk; Maund et al. 2013).

5.4 Implications for Type IIP SNe

Based on the cool temperatures originally assumed for the progenitors of SNe 2005cs (Maund et al. 2005; Li et al. 2006) and 2008bk (Mattila et al. 2008) (and the properties of the subsequent SNe), Pumo et al. (2009) suggested the progenitors may have been Super Asymptotic Giant Branch (SAGB) stars exploding as "electron capture" SNe (Nomoto 1984), rather than due to the collapse of an iron core. Our revised temperature for the progenitor of SN 2008bk clearly rules it out as being an SAGB star; and the new initial mass estimate suggests the progenitor was capable of producing an Fe-core at the end of its life.

The progenitor mass provides a key test of hydrodynamical models of SN evolution (specifically the behaviour of the light curve). For SN 2005cs there was a clear discrepancy between the progenitor mass determined from pre-explosion observations ($7 - 12M_{\odot}$ Maund et al. 2005; Li et al. 2006) and the hydrodynamical mass ($\sim 18M_{\odot}$ Utrobin & Chugai 2008). The recent reanalysis of the pre-explosion observations of SN 2005cs, using late-time observations (Maund et al. 2013) suggested the mass of the progenitor of SN 2005cs might be increased slightly ($\sim 1M_{\odot}$), but not enough to resolve the discrepancy. The increase in mass from our new analysis of the progenitor of SN 2008bk might go some way to resolve the discrepancy between the our progenitor masses and the hydrodynamical masses. Similarly, the revised mass estimate for this progenitor may suggest previous mass estimates for the progenitors of other Type IIP SNe have been underestimated. This may have contributed to the RSG problem (Smartt et al. 2009); however if the small increase in mass we have found for the progenitor of SN 2008bk were equally applicable to all progenitors, it would not completely eliminate the RSG problem. Although SN 2008bk was identified as a low-luminosity (low velocity, low Ni mass) Type IIP SN, the mass we derive for the progenitor is higher than previously determined for the progenitor of the similar SN 2005cs (Maund et al. 2013).

Maguire et al. (2012) analysed the nebular spectrum of SN 2008bk, and showed that the observed line fluxes were consistent with a model spectrum arising from a $12M_{\odot}$ progenitor, matching the result found here using pre-explosion observations. Recently, Jerkstrand et al. (2012) showed these line fluxes, in particular $[OI]$, could be used to establish the progenitor mass to within $\sim 3M_{\odot}$.

We note that the radius constraint for the progenitor of SN 2008bk presented here is at the lower end of the radius range of observed RSGs ($500 - 1500R_{\odot}$; see e.g. Massey & Olsen 2003; Levesque et al. 2007, 2006). Dessart et al. (2013) found, however, that RSGs with larger radii ($600 - 1100R_{\odot}$) would produce SN light curves with a U -band plateau before fading. To match the observed colour evolution of Type IIP SNe, they suggested the progenitors must be more compact stars; with radii similar to the radius we find for the progenitor of SN 2008bk.

5.5 The role of dust for the progenitors of Type IIP SNe

The dust responsible for the reddening of the progenitor of SN 2008bk most likely has a similar composition to interstellar dust (with an average $R_V = 3.1$ reddening law). The large reddenings inferred to nearby HII regions and the observation of a significant

light echo in HST observations (Van Dyk 2013), may suggest that the bulk of the reddening affecting the progenitor of SN 2008bk was in the ISM and not local to the star itself. The large amount of dust affecting the SED of the progenitor of SN 2008bk is, however, in conflict with the low reddening derived from the observations of SN 2008bk itself, in the analysis of Van Dyk et al. (2012); and is higher than estimated by Mattila et al. (2008) for their low mass solution.

Although dust has been suggested as a possible explanation for the RSG problem (Walmswell & Eldridge 2012; Kochanek et al. 2012), our analysis of the progenitor of SN 2008bk (and previous findings Maund et al. 2013) have not indicated that any CSM dust affecting the progenitors of Type IIP SNe have a different composition or reddening law compared to the ISM dust. While (Kochanek et al. 2012) suggested Silicate or Graphite dust might explain the observed SED of the progenitor of SN 2012aw, the available data for that progenitor is insufficient to rule out ordinary ISM dust. The conflicting reported reddening estimates to SN 2008bk itself (and towards objects in the vicinity in NGC 7793), derived from post-explosion observations, do not clarify if a large volume of dust in the CSM was destroyed by the SN (Dwek 1983; Pearce & Mayes 1986).

In the process of analysing the HST data, we note that we find disagreement between our photometry (presented in Table 3) and the photometry presented by Van Dyk (2013). In particular we find their $V-I$ colours to be too blue, being inconsistent with the optical and infrared colours predicted by MARCS spectra.

ACKNOWLEDGMENTS

The research of JRM is funded through a Royal Society University Research Fellowship.

References

- Alard, C. 2000, A&A Suppl., 144, 363
- Alard, C., & Lupton, R. H. 1998, ApJ, 503, 325
- Aldering, G., Humphreys, R. M., & Richmond, M. 1994, AJ, 107, 662
- Annibaldi, F., Aloisi, A., Mack, J., Tosi, M., van der Marel, R. P., Angeretti, L., Leitherer, C., & Sirianni, M. 2008, AJ, 135, 1900
- Appenzeller, I., et al. 1998, The Messenger, 94, 1
- Baron, E., et al. 2000, ApJ, 545, 444
- Bibby, J. L., & Crowther, P. A. 2010, MNRAS, 405, 2737
- Bohlin, R. C., & Gilliland, R. L. 2004, AJ, 127, 3508
- Cardelli, J. A., Clayton, G. C., & Mathis, J. S. 1989, ApJ, 345, 245
- Davies, B., et al. 2013, ArXiv e-prints
- Dessart, L., Hillier, D. J., Waldman, R., & Livne, E. 2013, MNRAS, 433, 1745
- Dolphin, A. E. 2000, PASP, 112, 1383
- Dwek, E. 1983, ApJ, 274, 175
- Ekström, S., et al. 2012, A&A, 537, A146
- Eldridge, J. J., & Tout, C. A. 2004, MNRAS, 353, 87
- Elias, J. H., Frogel, J. A., & Humphreys, R. M. 1985, ApJS, 57, 91
- Fraser, M., Maund, J. R., Smartt, S. J., Botticella, M.-T., Dall'Ora, M., Inserra, C., & et al. 2012, ArXiv e-prints
- Gilmozzi, R., Cassatella, A., Clavel, J., Gonzalez, R., & Fransson, C. 1987, Nature, 328, 318

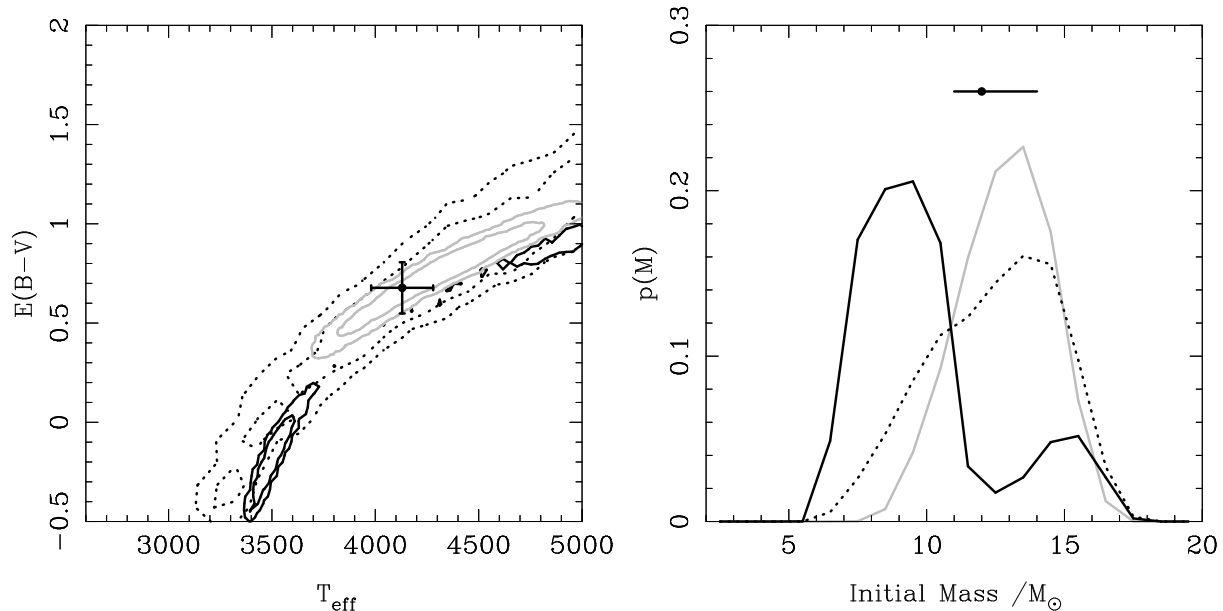


Figure 7. The properties of the progenitor derived from analysis of the photometry presented by Mattila et al. (2008) and Van Dyk et al. (2012). *Left*) The joint posterior distributions for $E(B-V)$ and T_{eff} given the datasets of Van Dyk et al. (solid contours) and Mattila et al. (dotted contours). The derived reddening and temperature from the analysis of Davies et al. (2013) is indicated by the point. *Right*) Mass probability density functions from analyses of the previous datasets (following the scheme of the left panel). For comparison our result, presented in Figure 6, is shown in grey.

- Gustafsson, B., Edvardsson, B., Eriksson, K., Jørgensen, U. G., Nordlund, Å., & Plez, B. 2008, *A&A*, 486, 951
- Hunter, I., et al. 2007, *A&A*, 466, 277
- Jacobs, B. A., Rizzi, L., Tully, R. B., Shaya, E. J., Makarov, D. I., & Makarova, L. 2009, *AJ*, 138, 332
- Jerkstrand, A., Fransson, C., Maguire, K., Smartt, S., Ergon, M., & Spyromilio, J. 2012, *A&A*, 546, A28
- Karachentsev, I. D., et al. 2003, *A&A*, 404, 93
- Kochanek, C. S., Khan, R., & Dai, X. 2012, *ApJ*, 759, 20
- Levesque, E. M., Massey, P., Olsen, K. A. G., & Plez, B. 2007, *ApJ*, 667, 202
- Levesque, E. M., Massey, P., Olsen, K. A. G., Plez, B., Meynet, G., & Maeder, A. 2006, *ApJ*, 645, 1102
- Li, W., Van Dyk, S. D., Filippenko, A. V., Cuillandre, J.-C., Jha, S., Bloom, J. S., Riess, A. G., & Livio, M. 2006, *ApJ*, 641, 1060
- Li, W., et al. 2008, *The Astronomer's Telegram*, 1448, 1
- Maguire, K., et al. 2012, *MNRAS*, 420, 3451
- Maoz, D., & Mannucci, F. 2008, *The Astronomer's Telegram*, 1464, 1
- Massey, P., & Olsen, K. A. G. 2003, *AJ*, 126, 2867
- Mattila, S., Smartt, S., Maund, J., Benetti, S., & Ergon, M. 2010, *ArXiv e-prints*
- Mattila, S., Smartt, S. J., Eldridge, J. J., Maund, J. R., Crockett, R. M., & Danziger, I. J. 2008, *ApJL*, 688, L91
- Maund, J., Reilly, E., & Mattila, S. 2013, *ArXiv e-prints*
- Maund, J. R., & Smartt, S. J. 2009, *Science*, 324, 486
- Maund, J. R., Smartt, S. J., & Danziger, I. J. 2005, *ArXiv Astrophysics e-prints astro-ph/0507502*
- Maund, J. R., Smartt, S. J., Kudritzki, R. P., Podsiadlowski, P., & Gilmore, G. F. 2004, *Nature*, 427, 129
- McCall, M. L., Rybski, P. M., & Shields, G. A. 1985, *ApJS*, 57, 1
- Monard, L. A. G. 2008, *Central Bureau Electronic Telegrams*, 1315, 1
- Morrell, N., & Stritzinger, M. 2008, *Central Bureau Electronic Telegrams*, 1335, 1
- Noeske, K., Baggett, S., Bushouse, H., Petro, L., Gilliland, R., & Khozurina-Platais, V. 2012, *WFC3 UVIS Charge Transfer Efficiency October 2009 to October 2011*, Tech. Rep. ISR WFC3 2012-09, Space Telescope Science Institute
- Nomoto, K. 1984, *ApJ*, 277, 791
- Pearce, G., & Mayes, A. J. 1986, *A&A*, 155, 291
- Pettini, M., & Pagel, B. E. J. 2004, *MNRAS*, 348, L59
- Pietrzyński, G., et al. 2010, *AJ*, 140, 1475
- Pilyugin, L. S., Vílchez, J. M., & Contini, T. 2004, *A&A*, 425, 849
- Pumo, M. L., et al. 2009, *ApJL*, 705, L138
- Schlaflly, E. F., & Finkbeiner, D. P. 2011, *ApJ*, 737, 103
- Skillington, J. 2004, in *American Institute of Physics Conference Series*, Vol. 735, American Institute of Physics Conference Series, ed. R. Fischer, R. Preuss, & U. V. Toussaint, 395–405
- Smartt, S. J. 2009, *ARAA*, 47, 63
- Smartt, S. J., Eldridge, J. J., Crockett, R. M., & Maund, J. R. 2009, *MNRAS*, 395, 1409
- Utrobin, V. P., & Chugai, N. N. 2008, *A&A*, 491, 507
- Van Dyk, S. D. 2013, *ArXiv e-prints*
- Van Dyk, S. D., et al. 2012, *AJ*, 143, 19
- Walmswell, J. J., & Eldridge, J. J. 2012, *MNRAS*, 419, 2054
- Westera, P., Lejeune, T., Buser, R., Cuisinier, F., & Bruzual, G. 2002, *A&A*, 381, 524